© SEP 2026 | IRE Journals | Volume 10 Issue 3 | ISSN: 2456-8880
DOI: https://doi.org/10.64388/IREV10I3-1723302

EDTA-Functionalized MgO as a High-Performance Electrode Material for Supercapacitor Applications

LALIT N. PATIL[1], MADHUKAR G. KASAR[2*]
[1]*Deparment of chemistry, ACS College Taloda. (M.S.), Dist- Nandurbar (MS), India*
[2*]*Deparment of chemistry, Smt. N. N. C. Arts Commerce and Science college Kusumba, Tal-Dist Dhule (M.S.), India*

Abstract- ***The increasing demand for efficient and sustainable energy-storage systems has stimulated the development of advanced electrode materials for supercapacitor applications. In the present work, ethylenediaminetetraacetic acid-functionalized magnesium oxide (EDTA@MgO) was developed as a surface-modified electrode material to improve the electrochemical performance of pristine MgO. MgO was synthesized through a precipitation-assisted ultrasonication method followed by calcination, while EDTA functionalization was subsequently employed to modify its surface properties. The structural, functional, morphological, and optical characteristics of the prepared materials were investigated using XRD, FTIR, FE-SEM, and UV–Visible spectroscopy. XRD analysis confirmed the crystalline cubic structure of MgO, whereas FTIR results supported the successful interaction of EDTA with the MgO surface. FE-SEM analysis revealed a hierarchical agglomerated morphology for MgO and noticeable surface modification with layered features after functionalization. Electrochemical investigations demonstrated the superior performance of EDTA@MgO compared with pristine MgO. The EDTA@MgO electrode exhibited an enhanced CV response, reduced impedance characteristics, and improved charge-storage capability. A specific capacitance of 356.22 F g^{-1} at 10 mV s^{-1} was obtained from CV analysis, while a higher specific capacitance of 507.26 F g^{-1} at 1 A g^{-1} was achieved from GCD measurements. The improved performance is attributed to enhanced electrolyte interaction and increased accessibility of electrochemically active sites following EDTA functionalization. These findings demonstrate the potential of EDTA@MgO as a promising electrode material for supercapacitor applications.***

Keywords: EDAT, MgO, Supercapacitor, metal oxide

I. INTRODUCTION

The rapidly growing demand for portable electronics, electric transportation, and renewable energy integration has intensified the need for efficient and sustainable energy-storage systems [1]. Electrochemical energy-storage devices are particularly attractive because of their high efficiency, operational flexibility, and ability to support modern energy infrastructure [2]. Among these devices, supercapacitors have received considerable attention owing to their high power density, rapid charge-discharge capability, and excellent cycling stability [3]. Unlike batteries, which generally store energy through relatively slow bulk Faradaic reactions and offer high energy density, supercapacitors store charge through electrical double-layer formation and/or rapid reversible surface redox reactions [4]. Consequently, supercapacitors can deliver energy much faster and withstand a significantly larger number of charge-discharge cycles, although their energy density is generally lower than that of batteries [5].

The electrochemical performance of supercapacitors strongly depends on the properties of electrode materials. Carbon-based materials provide excellent electrical conductivity and electrical double-layer charge storage, whereas metal oxides offer high theoretical capacitance, chemical stability, abundant electroactive sites, and reversible Faradaic charge-storage behaviour [6, 7]. Nanostructured metal oxides are particularly advantageous because their large surface area and shortened ion-diffusion pathways facilitate electrolyte accessibility and rapid electrochemical reactions [8]. However, their practical application is often limited by poor intrinsic electrical conductivity, particle agglomeration, and relatively slow charge-transfer kinetics. Therefore, surface functionalization and composite formation have emerged as effective approaches for improving their electrochemical performance [9].

Magnesium oxide (MgO) is a promising metal oxide because of its low cost, chemical and thermal stability, environmental compatibility, and versatile surface properties [10]. However, the limited electrical

conductivity of pristine MgO restricts its direct electrochemical performance. Surface modification with functional molecules can provide an effective route to improve electrolyte interaction and increase the accessibility of surface-active sites[11]. Ethylenediaminetetraacetic acid (EDTA), a multifunctional chelating molecule containing nitrogen- and oxygen-rich functional groups, can interact strongly with metal-containing surfaces. Its incorporation with MgO can modify surface chemistry, improve dispersion, enhance electrolyte wettability, and promote ion transport at the electrode-electrolyte interface [12].

Previous studies have demonstrated that combining metal oxides with functional organic components or conducting polymers can significantly improve supercapacitor performance [13, 14]. Conducting polymers such as polyaniline and polypyrrole provide high electrical conductivity and additional pseudocapacitive redox sites, thereby improving electron transport and charge-storage capability [15]. Their integration with metal oxides can create synergistic composites in which the metal oxide provides structural stability while the polymer facilitates electronic conduction and reversible charge storage. Such hybrid material design represents an effective strategy for overcoming the limitations of individual electrode components [16, 17].

Electrochemical techniques provide the most direct and reliable approach for evaluating the energy-storage behavior of newly developed electrode materials [18]. Cyclic voltammetry is used to investigate charge-storage mechanisms and reversibility, galvanostatic charge-discharge measurements determine capacitance and energy-storage performance, while electrochemical impedance spectroscopy provides information regarding internal resistance and charge-transfer kinetics [19-21]. Together, these methods establish the relationship between material properties and practical electrochemical performance.

The development of low-cost, stable, and environmentally compatible electrode materials also has important social and technological significance. Advanced supercapacitors can support renewable-energy storage, electric mobility, portable electronics, and efficient power-management systems [22]. Therefore, the utilization of abundant materials such as MgO combined with effective surface functionalization offers a potentially sustainable approach toward advanced energy-storage technologies.

In the present work, an EDTA-functionalized magnesium oxide nanocomposite (EDTA@MgO) was developed and investigated as a potential electrode material for supercapacitor applications. The functionalization of MgO with EDTA was designed to modify its surface properties, improve electrolyte interaction, and enhance electrochemical charge-storage behavior. The structural and physicochemical characteristics of the prepared nanocomposite were investigated, followed by detailed electrochemical evaluation using cyclic voltammetry, galvanostatic charge-discharge, and electrochemical impedance spectroscopy. This work highlights the potential of organic-functionalized metal oxide nanocomposites as promising materials for efficient and sustainable supercapacitor applications.

II. MATERIALS AND METHODS

2.1. Materials

$Mg(NO_3)_2$ and NaOH were used as the precursor and precipitating agent, respectively. NH_4OH was also used as an alternative precipitating agent for comparison. Ethanol and DD water were used during the synthesis and washing processes. All chemicals were of analytical grade and used without further purification.

2.2. Synthesis of MgO Nanomaterial

MgO particles were synthesized using a precipitation-assisted ultrasonication method followed by calcination. Initially, a 0.2 M solution of $Mg(NO_3)_2$ was prepared in 100 mL of DD water and transferred to a 250 mL beaker. Subsequently, a 0.4 M NaOH solution was added dropwise to the $Mg(NO_3)_2$ solution under continuous ultrasonication. The molar ratio of Mg^{2+} ions to OH^- ions was maintained at 1:2. The resulting mixture was further ultrasonicated for 2 h at room temperature to facilitate the formation of $Mg(OH)_2$ and minimize particle agglomeration. The precipitation reaction is represented by Eq. (1):

$$Mg(NO_3)_2 + 2NaOH \rightarrow Mg(OH)_2 + 2NaNO_3 \quad (1)$$

The resulting $Mg(OH)_2$ precipitate was collected by filtration and thoroughly washed with DD water to remove residual impurities. Ethanol was subsequently added, and the obtained sample was dried at 110 °C for 24 h. The dried precursor was then calcined at 500 °C for 4 h to obtain hierarchically structured MgO particles. The thermal decomposition of $Mg(OH)_2$ is represented by Eq. (2):

$$Mg(OH)_2 \rightarrow MgO + H_2O \qquad (2)$$

For comparison, MgO particles were also synthesized using NH_4OH as the precipitating agent instead of NaOH. The same experimental procedure and reaction conditions were maintained. In this case, $Mg(OH)_2$ was formed according to Eq. (3):

$$Mg(NO_3)_2 + 2NH_4OH \rightarrow Mg(OH)_2 + 2NH_4NO_3 \quad (3)$$

The resulting $Mg(OH)_2$ precursor was subsequently washed, dried, and calcined under identical conditions to obtain MgO:

$$Mg(OH)_2 \rightarrow MgO + H_2O \qquad (4)$$

The MgO particles synthesized using NaOH and NH_4OH were subsequently used for further surface modification and electrochemical investigations.

2.3. Synthesis of EDTA@MgO Nanocomposite

The EDTA@MgO nanocomposite was prepared by a simple surface-functionalization method. A predetermined amount of the synthesized MgO was dispersed in DD water under continuous stirring and ultrasonication to obtain a homogeneous suspension. Separately, an appropriate amount of EDTA was dissolved in DD water and added dropwise to the MgO suspension under continuous stirring. The reaction mixture was further stirred for a sufficient period to promote the interaction of EDTA with the MgO surface.

The resulting product was collected by filtration, washed repeatedly with DD water to remove unreacted EDTA and other impurities, and subsequently dried at an appropriate temperature. The dried product was gently ground to obtain the EDTA@MgO nanocomposite, which was further used for characterization and electrochemical studies.

2.4. Material Characterization

The structural and physicochemical properties of MgO and EDTA@MgO were investigated using various characterization techniques. The crystalline structure and phase purity of the prepared materials were examined using X-ray diffraction (XRD). The functional groups and interaction between EDTA and MgO were investigated using Fourier-transform infrared spectroscopy (FTIR). The surface morphology and microstructural characteristics were analyzed using scanning electron microscopy (SEM).

The optical properties of the prepared materials were investigated using ultraviolet-visible spectroscopy (UV-Vis). The electrochemical surface properties and charge-storage behavior were subsequently evaluated using CHI-660C electrochemical techniques.

2.5. Electrode Preparation

The working electrode was prepared by mixing EDTA@MgO, carbon black, and PVDF in a weight ratio of 8:1:1 to obtain a homogeneous slurry. The prepared slurry was uniformly coated onto Ni foam (1 × 1 cm), which served as the current collector. The coated electrode was subsequently dried to remove the solvent and improve the adhesion of the active material to the Ni foam. The prepared electrode was pressed, where necessary, to ensure good contact and mechanical stability between the active material and the current collector. The resulting EDTA@MgO-coated Ni foam electrode was subsequently used as the working electrode for electrochemical measurements. The mass of active material deposited on the electrode was carefully measured before electrochemical analysis. The prepared EDTA@MgO electrode was then used as the working electrode for electrochemical measurements.

2.6. Electrochemical Measurements

The electrochemical performance of the prepared electrode was investigated using a conventional three-electrode system at room temperature. The EDTA@MgO-coated electrode was used as the working electrode, while suitable reference and counter electrodes were employed. An aqueous electrolyte solution was used as the supporting electrolyte.

The electrochemical behavior of the electrode was evaluated using cyclic voltammetry (CV),

© SEP 2026 | IRE Journals | Volume 10 Issue 3 | ISSN: 2456-8880
DOI: https://doi.org/10.64388/IREV10I3-1723302

galvanostatic charge-discharge (GCD), and electrochemical impedance spectroscopy (EIS). CV measurements were performed at different scan rates to investigate the charge-storage mechanism and electrochemical reversibility of the electrode. GCD measurements were carried out at different current densities to determine the specific capacitance, energy density, power density, and rate capability. EIS measurements were performed over an appropriate frequency range to evaluate the internal resistance and charge-transfer characteristics of the electrode.

The specific capacitance was calculated from the GCD curves using Eq. (5):

$$C_s = \frac{I\Delta t}{m\Delta V} \qquad (5)$$

where C_s is the specific capacitance, I is the discharge current, Δt is the discharge time, m is the mass of electroactive material, and ΔV is the potential window.

III. CHARACTERIZATION

3.1. X-Ray Diffraction

The structural characteristics and phase composition of MgO and EDTA@MgO were investigated using XRD analysis, as shown in Fig. 1 a, b. The diffraction pattern of MgO exhibited distinct diffraction peaks at 2θ values of 36.92°, 42.92°, 62.27°, 74.73°, and 78.61°, corresponding to the (111), (200), (220), (311), and (222) crystallographic planes, respectively. These characteristic reflections confirm the formation of crystalline MgO with a cubic crystal structure. The XRD pattern of EDTA@MgO also exhibited the characteristic diffraction reflections associated with MgO, confirming that the fundamental crystalline structure of MgO was retained after functionalization. However, noticeable variations in peak intensity and peak broadening were observed compared with pristine MgO. In addition, the modified diffraction profile indicates the influence of EDTA incorporation on the surface and structural characteristics of MgO. The observed changes may be associated with the interaction between EDTA functional groups and the MgO surface, resulting in modifications to crystallite growth and the overall diffraction behavior of the material.

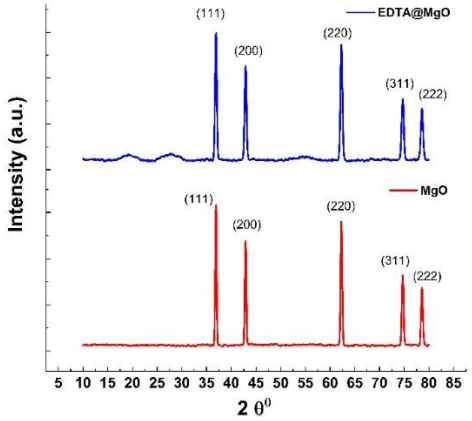

Figure.1. X-Ray Diffraction patterns of MgO and EDTA@MgO

The preservation of the characteristic MgO diffraction peaks in EDTA@MgO indicates that EDTA functionalization did not completely disrupt the crystalline MgO framework. The structural modification introduced by EDTA is expected to influence the surface properties, electrolyte interaction, and electrochemical charge-storage behavior of the material. Thus, the XRD results demonstrate the successful formation of MgO and the structural modification of MgO following EDTA functionalization, supporting its potential application as an electrode material for supercapacitor applications.

3.2. Spectroscopic Characterization

3.2.1. FTIR Spectra

The FTIR spectra of MgO and EDTA@MgO were recorded to investigate the surface functional groups and confirm the interaction between EDTA and MgO, as shown in Fig. 2. The spectrum of pristine MgO exhibited a broad absorption band centered at approximately 3197.97 cm^{-1}, which can be attributed to the stretching vibration of surface-adsorbed hydroxyl groups and physically adsorbed water molecules. The absorption band at 1615.30 cm^{-1} is associated with the bending vibration of adsorbed water molecules. The bands observed at approximately 3968.91 and 3732.32 cm^{-1} can be assigned to surface hydroxyl species. The absorption feature at 1036.08 cm^{-1} may be related to surface carbonate or hydroxyl-associated vibrations resulting from atmospheric adsorption. Furthermore, the band observed at approximately 675.08 cm^{-1} is attributed to

the characteristic Mg–O lattice vibration, confirming the formation of MgO.

Material	Observed band (cm^{-1})	Possible assignment
MgO	3968.91	Surface hydroxyl stretching vibration
MgO	3732.32	Surface –OH stretching vibration
MgO	3197.97	Broad O–H stretching of adsorbed water/surface hydroxyl groups
MgO	1615.30	H–O–H bending vibration of adsorbed water
MgO	1036.08	Surface carbonate and/or hydroxyl-associated vibration
MgO	675.08	Mg–O lattice vibration
EDTA@MgO	3744.56	Surface O–H stretching vibration
EDTA@MgO	1649.97	Asymmetric stretching of carboxylate groups
EDTA@MgO	1501.07	Carboxylate-related vibration and interaction with MgO surface
EDTA@MgO	1164.57	C–N and/or C–O stretching vibration associated with EDTA
EDTA@MgO	805.61	Mg–O vibration and/or surface-functionalized structural vibration

Table-1. FTIR Spectra for MgO and EDTA@MgO

In the EDTA@MgO spectrum, significant changes in the absorption profile were observed compared with pristine MgO, confirming the surface modification of MgO by EDTA. The characteristic band at approximately 1649.97 cm^{-1} is attributed to the asymmetric stretching vibration of carboxylate groups associated with EDTA. The band observed at 1501.07 cm^{-1} may be assigned to carboxylate-related vibrations and interactions between the EDTA functional groups and the MgO surface. The absorption band at approximately 1164.57 cm^{-1} is associated with C–N and/or C–O stretching vibrations originating from the EDTA structure. The band observed near 805.61 cm^{-1} can be associated with Mg–O vibrations and overlapping vibrations of the surface-functionalized structure. In addition, the absorption band at 3744.56 cm^{-1} corresponds to surface hydroxyl stretching vibrations.

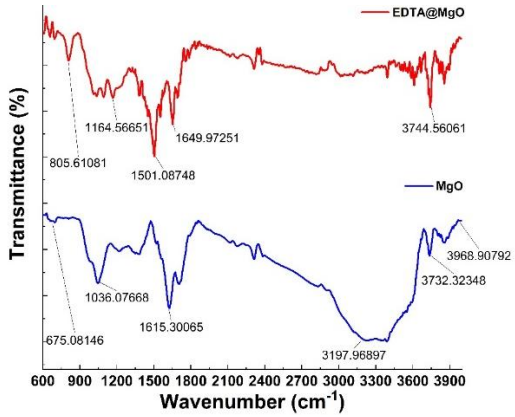

Figure 2. FTIR Spectra of MgO and EDTA@MgO

The appearance and modification of the characteristic carboxylate- and nitrogen-containing functional group vibrations in EDTA@MgO, together with changes in the MgO absorption profile, support the successful interaction of EDTA with the MgO surface. These surface functional groups are expected to improve the surface chemistry and electrolyte interaction of EDTA@MgO, which may contribute to its enhanced electrochemical behavior.

3.2.2. UV-Visible Sepectra

The UV–Visible absorption spectra of MgO and EDTA@MgO were recorded in the wavelength range of 200–900 nm to investigate their optical absorption characteristics, as shown in Fig. 3. The x-axis should

be labeled as Wavelength (nm), rather than Wavenumber (cm^{-1}), because the spectrum is recorded in the 200–900 nm range.

The MgO sample exhibited a characteristic absorption maximum at approximately 286.6 nm, along with an absorption feature near 265.4 nm. The absorption in the ultraviolet region is associated with the electronic transitions and intrinsic optical properties of MgO. The strong absorption edge observed in the UV region confirms the wide-band-gap nature of the synthesized MgO material.

After EDTA functionalization, the absorption maximum showed a slight shift to approximately 287.8 nm. This change in the absorption behavior indicates the interaction of EDTA with the MgO surface and modification of the electronic environment of the material. The slight shift in the absorption maximum may be attributed to surface functionalization and the interaction between the functional groups of EDTA and MgO. Moreover, the variation in the overall absorption profile of EDTA@MgO compared with pristine MgO further supports the successful surface modification of MgO.

The observed changes in the UV–Visible absorption characteristics are consistent with the FTIR results, indicating that EDTA incorporation influenced the surface and electronic properties of MgO without causing a major alteration in its fundamental optical characteristics. Such modification of the surface electronic environment may facilitate improved interaction with the electrolyte and contribute to enhanced electrochemical behavior in supercapacitor applications.

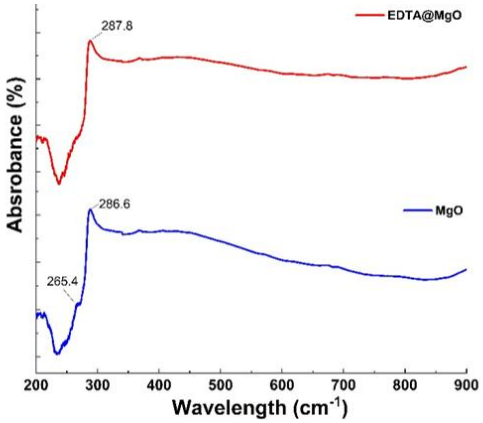

Figure 3. UV-Visible Spectra of MgO and EDTA@MgO

Table-2. UV-Visible Bands for MgO and EDTA@MgO

Material	*Absorption feature (nm)*	*Observation*	*Possible interpretation*
MgO	*265.4*	*Absorption feature/shoulder*	*Intrinsic electronic transition or surface-related absorption*
MgO	*286.6*	*Main absorption maximum*	*Characteristic UV absorption of MgO*
EDTA@MgO	*287.8*	*Main absorption maximum*	*Modified electronic environment after EDTA functionalization*
EDTA@MgO	*~200–300*	*Broad UV absorption region*	*Contribution from MgO and EDTA-induced surface modification*

3.3. Morphological Characterization

3.3.1. FE-SEM analysis

The surface morphology and microstructural characteristics of the synthesized MgO and EDTA@MgO were investigated using field-emission scanning electron microscopy (FE-SEM), as shown in Fig. 4a and b. The FE-SEM images reveal a noticeable difference in the surface morphology of the material before and after EDTA functionalization, indicating the influence of surface modification on particle organization and morphology.

© SEP 2026 | IRE Journals | Volume 10 Issue 3 | ISSN: 2456-8880
DOI: https://doi.org/10.64388/IREV10I3-1723302

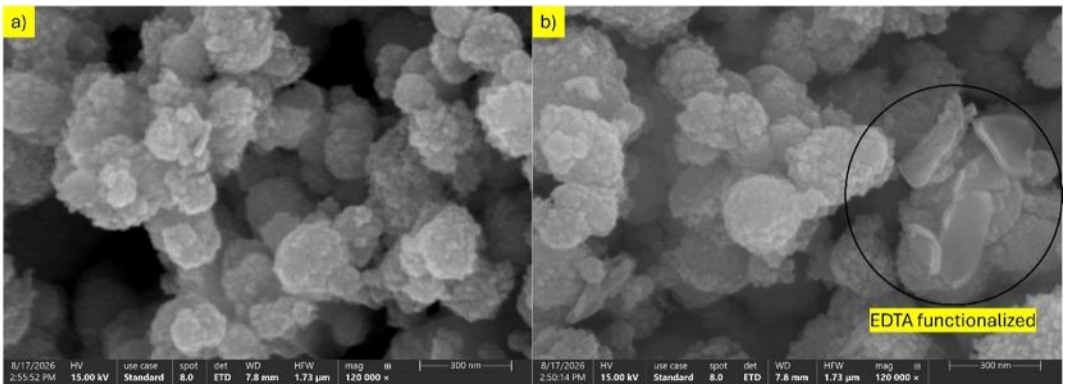

Figure 4. FE-SEM images of (a) pristine MgO and (b) EDTA@MgO

The pristine MgO sample shown in Fig. 4a exhibits an irregular, highly agglomerated morphology composed of interconnected nanoscale particles. The particles appear to assemble into larger hierarchical clusters with a rough and heterogeneous surface. Several agglomerates possess a cauliflower-like or flower-like appearance, resulting from the assembly of smaller primary particles. Such agglomeration is commonly associated with the high surface energy of nanosized oxide particles. The hierarchical arrangement of the MgO particles can provide surface roughness and interconnected void spaces, which may increase the accessible surface area and facilitate electrolyte penetration during electrochemical operation. However, excessive particle agglomeration may reduce the availability of individual active sites and limit efficient ion diffusion.

In comparison, the EDTA@MgO sample shown in Fig. 4b displays a significantly modified surface morphology. Although the hierarchical and aggregated nature of MgO is retained, the surface of the particles appears to exhibit additional irregular and layered features after EDTA functionalization. Particularly, the highlighted region shows the presence of relatively smooth plate-like or sheet-like structures associated with the MgO aggregates. These morphological changes suggest that EDTA functionalization influenced the surface growth and assembly of MgO particles. The interaction between the functional groups of EDTA and surface Mg sites may alter particle-particle interactions and lead to the observed modification in the surface texture.

The appearance of the plate-like and layered features in EDTA@MgO may also indicate the formation of a surface-associated EDTA-rich layer or the rearrangement of MgO particles following functionalization. Importantly, the coexistence of rough hierarchical aggregates and relatively smooth surface regions may generate a heterogeneous surface architecture with improved interfacial characteristics. Such a structure can potentially provide additional electrolyte-accessible regions and facilitate interactions between the electrode material and electrolyte ions.

Furthermore, the modified morphology of EDTA@MgO suggests improved structural complexity compared with pristine MgO. The rough and interconnected architecture can provide pathways for electrolyte-ion diffusion, while EDTA-induced surface modification may enhance the surface wettability and accessibility of electrochemically active sites. The presence of functional groups associated with EDTA, as supported by the FTIR analysis, together with the observed morphological modification, confirms the successful surface engineering of MgO.

3.4. Electrochemical Characterization

Fig. 5a compares the CV profiles of MgO and EDTA@MgO electrodes. Both electrodes exhibit nonlinear CV curves, indicating that the charge-storage process involves contributions beyond ideal electric double-layer capacitance. However, the EDTA@MgO electrode displays a significantly larger enclosed CV area and higher current response than pristine MgO, demonstrating its improved charge-storage capability. The enhanced electrochemical response of EDTA@MgO can be attributed to the surface functionalization of MgO by EDTA. The

© SEP 2026 | IRE Journals | Volume 10 Issue 3 | ISSN: 2456-8880
DOI: https://doi.org/10.64388/IREV10I3-1723302

presence of oxygen- and nitrogen-containing functional groups may improve the interaction between the electrode surface and electrolyte ions, thereby providing additional electrochemically accessible sites. Furthermore, the modified surface architecture observed in FE-SEM may facilitate electrolyte penetration and ion transport. The larger current response and enclosed area of EDTA@MgO therefore suggest a higher capacitance and improved electrochemical activity compared with pristine MgO.

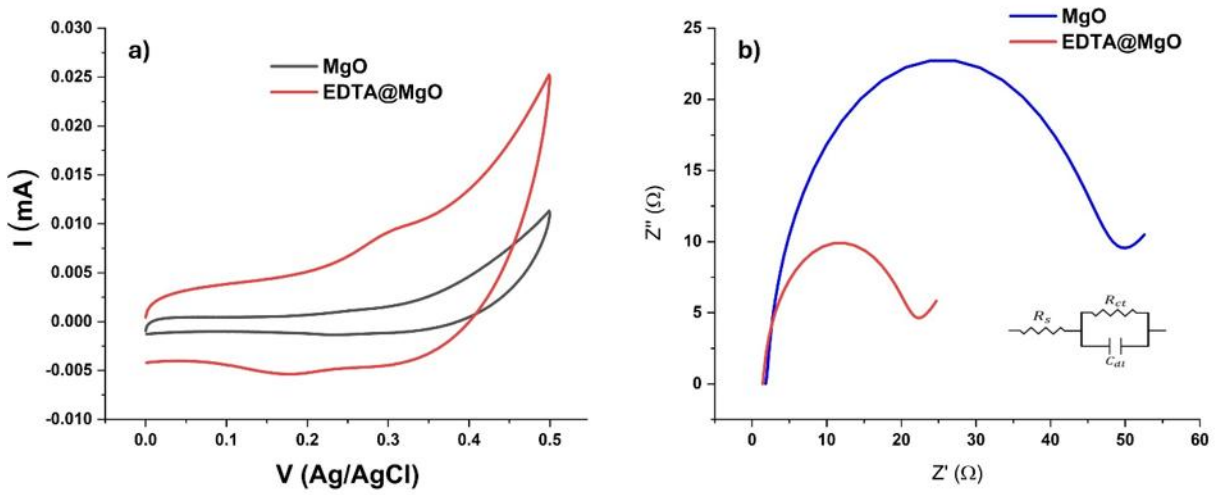

Figure 5. a) CV and b) EIS spectra of MgO and EDTA@MgO

The EIS results are presented as Nyquist plots in Fig. 5b. The spectra show a high-frequency semicircular region followed by a low-frequency tail, representing the combined effects of charge-transfer resistance (R_{CT}= 56 Ω and ion-diffusion behavior. A smaller semicircle generally indicates lower charge-transfer resistance and faster electron-transfer kinetics at the electrode-electrolyte interface.

In the present plot, however, the EDTA@MgO curve shows a smaller semicircular response and lower overall impedance than MgO, indicating improved charge-transfer characteristics (R_{CT} = 24 Ω) after EDTA functionalization. The lower resistance can facilitate faster electron transport and more efficient electrolyte-ion movement within the electrode structure. The improved interfacial properties of EDTA@MgO may arise from the modified surface chemistry and enhanced electrode-electrolyte interaction provided by EDTA functionalization.

IV. SUPERCAPACITOR STUDIES

The electrochemical performance of the EDTA@MgO electrode was investigated using CV, GCD, and EIS measurements, as illustrated in Fig. 6a–d. The combined results demonstrate the charge-storage behavior, rate capability, and electrochemical response of the EDTA-functionalized MgO electrode.

© SEP 2026 | IRE Journals | Volume 10 Issue 3 | ISSN: 2456-8880
DOI: https://doi.org/10.64388/IREV10I3-1723302

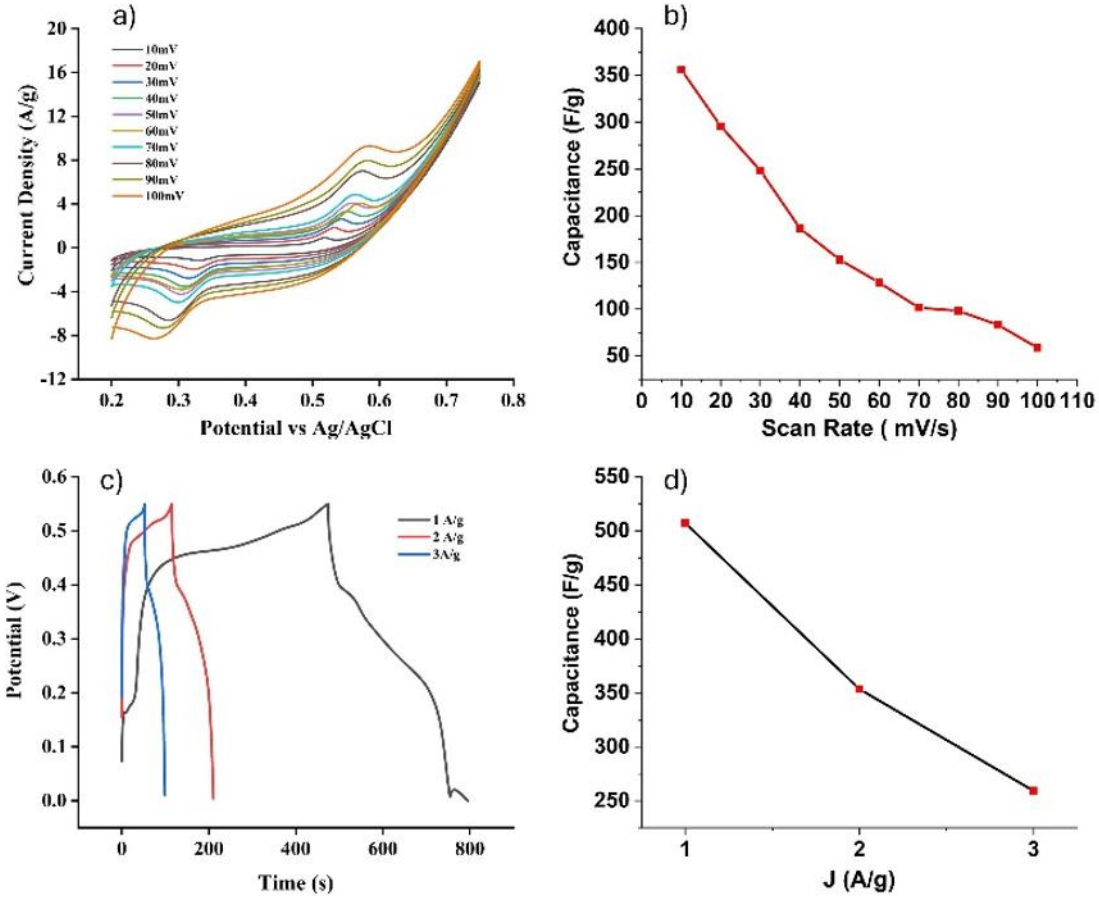

Figure 6. a) CV, b) Capacitance Vs Scan Rate, c) GCD and d) Capacitance Vs Current Density plot of EDTA@MgO

Fig. 6a presents the CV curves of the EDTA@MgO electrode recorded at scan rates ranging from 10 to 100 mV s^{-1}. The CV curves exhibit nonlinear profiles with broad anodic and cathodic features, indicating that the charge-storage mechanism involves a combination of capacitive and Faradaic contributions rather than purely electric double-layer charge storage. With increasing scan rate, the current density and enclosed area of the CV curves increase considerably, demonstrating the rapid electrochemical response of the electrode. Although slight distortion is observed at higher scan rates because of polarization and limited ion-diffusion time, the overall electrochemical response is maintained. The specific capacitance calculated from the CV data was 356.22 F g^{-1} at 10 mV s^{-1}, confirming the considerable charge-storage capability of EDTA@MgO. The favorable CV response can be attributed to the EDTA-induced surface functionalization, which provides oxygen- and nitrogen-containing functional groups and improves electrode-electrolyte interaction and accessibility of electrochemically active sites.

The variation of specific capacitance with scan rate is shown in Fig. 6b. The capacitance decreases progressively as the scan rate increases. This behavior is associated with the limited accessibility of internal electrochemically active sites at higher scan rates. At lower scan rates, electrolyte ions have sufficient time to penetrate the electrode structure and interact with a larger number of active sites, resulting in higher capacitance. Conversely, at higher scan rates, the rapid potential sweep restricts ion diffusion, and charge storage predominantly occurs at easily accessible surface sites. The gradual decrease in capacitance therefore reflects the kinetic limitations associated with ion transport while also providing information regarding the rate capability of the EDTA@MgO electrode.

Fig. 6c shows the GCD curves of the EDTA@MgO electrode recorded at current densities of 1, 2, and 3 A g^{-1}. The curves exhibit nonlinear and asymmetric charge-discharge profiles rather than ideal triangular shapes, indicating the contribution of pseudocapacitive or surface-controlled Faradaic processes to the overall charge-storage mechanism. The discharge time decreases with increasing current density, which is expected because the charge-discharge process occurs more rapidly at higher applied currents. The EDTA@MgO electrode exhibits the longest discharge duration at 1 A g^{-1}, indicating greater utilization of electrochemically active sites under slower charge-discharge conditions.

The specific capacitance calculated from the GCD curves was 507.26 F g^{-1} at 1 A g^{-1}, as shown in Fig. 6d. The capacitance decreases with increasing current density, reaching approximately 355 F g^{-1} at 2 A g^{-1} and 260 F g^{-1} at 3 A g^{-1}. The reduction in capacitance at higher current densities can be attributed to insufficient time for complete electrolyte-ion diffusion and limited utilization of less accessible active sites. At lower current density, electrolyte ions can effectively penetrate the electrode structure and participate in charge-storage processes, leading to a higher capacitance value.

The difference between the capacitance values obtained from CV (356.22 F g^{-1} at 10 mV s^{-1}) and GCD (507.26 F g^{-1} at 1 A g^{-1}) arises from differences in the electrochemical measurement methods and calculation procedures. CV evaluates the integrated current response over a selected potential window and scan rate, whereas GCD capacitance is calculated from the discharge time under a constant applied current. Therefore, different capacitance values obtained using these techniques are expected and provide complementary information regarding the charge-storage behavior of the electrode.

CONCLUSION

In this work, MgO was successfully synthesized through precipitation followed by calcination and subsequently surface-functionalized with EDTA to obtain the EDTA@MgO electrode material. The characterization results confirmed the successful structural and surface modification of MgO. XRD analysis demonstrated the retention of the characteristic crystalline structure of MgO after functionalization, while FTIR revealed changes associated with EDTA-derived functional groups and their interaction with the MgO surface. FE-SEM observations further showed noticeable morphological modifications, including heterogeneous and layered surface features in EDTA@MgO.

Electrochemical studies demonstrated that EDTA functionalization significantly improved the charge-storage behavior of MgO. The EDTA@MgO electrode exhibited a larger CV response and improved impedance characteristics compared with pristine MgO, indicating enhanced electrode-electrolyte interaction and charge-transfer behavior. The electrode delivered a specific capacitance of 356.22 F g^{-1} at 10 mV s^{-1} from CV analysis and 507.26 F g^{-1} at 1 A g^{-1} from GCD analysis. The decrease in capacitance at higher scan rates and current densities was attributed to limitations in electrolyte-ion diffusion and the reduced accessibility of internal active sites during rapid charge-discharge processes.

REFERENCES

[1] Njema, G.G., R.B.O. Ouma, and J.K. Kibet, A review on the recent advances in battery development and energy storage technologies. *Journal of renewable energy*, 2024. 2024(1): p. 2329261. Wiley

[2] Venkatesan, S.V., et al., Recent advances in the unconventional design of electrochemical energy storage and conversion devices. *Electrochemical Energy Reviews*, 2022. 5(4): p. 16. Springer

[3] Wang, F., et al., Latest advances in supercapacitors: from new electrode materials to novel device designs. *Chemical Society Reviews*, 2017. 46(22): p. 6816-6854. Royal Society of Chemistry

[4] Conway, B.E., Transition from "supercapacitor" to "battery" behavior in electrochemical energy storage. *Journal of the Electrochemical Society*, 1991. 138(6): p. 1539-1548. IOPscience

[5] Shao, Y., et al., Design and mechanisms of asymmetric supercapacitors. *Chemical reviews*, 2018. 118(18): p. 9233-9280. ACS

[6] Zhi, M., et al., Nanostructured carbon–metal oxide composite electrodes for supercapacitors: a review. *Nanoscale*, 2012. 5(1): p. 72-88.

[7] Tundwal, A., et al., Developments in conducting polymer-, metal oxide-, and carbon nanotube-based composite electrode materials for supercapacitors: a review. *RSC advances*, 2024. 14(14): p. 9406-9439. Royal Society of Chemistry

[8] Jiang, J., et al., Recent advances in metal oxide-based electrode architecture design for electrochemical energy storage. *Advanced materials*, 2012. 24(38): p. 5166-5180. Wiley

[9] Hussain, M.D., et al., Advancement in metal organic frameworks@ metal oxides composites for energy and environmental applications. *Environmental Progress & Sustainable Energy*, 2025. 44(6): p. e70104. Wiley

[10] Mahiba, G.G.J., A. Prabakaran, and B. Balraj, A review on multifunctional applications of MgO nanostructures: from material science to environmental and agricultural innovations. *RSC advances*, 2026. 16(15): p. 13040-13061. Royal Society of Chemistry

[11] Kaseem, M., et al., Chemisorption-dominated organic–silicate hybrid anchoring on porous MgO for durable corrosion protection of AZ31 Mg alloy. *Journal of Magnesium and Alloys*, 2026: p. 102177. Crossref

[12] Goyal, M., S.K. Pandey, and N. Bhatnagar, Synergistic experimental and computational study of Zn and Cd doped PEDOT: PSS/MgO nanocomposites for enhanced supercapacitor performance. *Scientific Reports*, 2026. Nature

[13] Patil, P.H., V.V. Kulkarni, and S.A. Jadhav, An overview of recent advancements in conducting polymer–metal oxide nanocomposites for supercapacitor application. *Journal of Composites Science*, 2022. 6(12): p. 363. MDPI

[14] Annu, et al., Unraveling the electrochemical insights of cobalt oxide/conducting polymer hybrid materials for supercapacitor, battery, and supercapattery applications. *Polymers*, 2024. 16(20): p. 2907. MDPI

[15] Heydari Gharahcheshmeh, M. and K. Chowdhury, Fabrication methods, pseudocapacitance characteristics, and integration of conjugated conducting polymers in electrochemical energy storage devices. *Energy Advances*, 2024. 3(11): p. 2668-2703. Royal Society of Chemistry

[16] Aldukhayel, A.M., Metal Oxide-Polymer Hybrid Materials for Advanced Energy Applications. *Journal of Inorganic and Organometallic Polymers and Materials*, 2026: p. 1-19. Crossref

[17] Akhtar, M., et al., Metal oxide-polymer hybrid composites: a comprehensive review on synthesis and multifunctional applications. *RSC advances*, 2025. 15(23): p. 18173-18208. Royal Society of Chemistry

[18] Talaie, E., et al., Methods and protocols for electrochemical energy storage materials research. *Chemistry of Materials*, 2017. 29(1): p. 90-105. ACS

[19] Qu, D., et al., Electrochemical impedance and its applications in energy-storage systems. *Small Methods*, 2018. 2(8): p. 1700342. Wiley

[20] Mathis, T.S., et al., Energy storage data reporting in perspective—guidelines for interpreting the performance of electrochemical energy storage systems. *Advanced Energy Materials*, 2019. 9(39): p. 1902007. Wiley

[21] Fleischmann, S., et al., Pseudocapacitance: from fundamental understanding to high power energy storage materials. *Chemical Reviews*, 2020. 120(14): p. 6738-6782. ACS

[22] Salaheldeen, M., et al., Empowering the future: cutting-edge developments in supercapacitor technology for enhanced energy storage. *Batteries*, 2025. 11(6): p. 232. MDPI